High-resolution chemostratigraphy of the Cambrian−Ordovician GSSP: enhanced global correlation tool

Karem Azmy[a*], Svend Stouge[b], Uwe Brand[c], Gabriella Bagnoli[d], Robert Ripperdan[e]

[a] Department of Earth Sciences, Memorial University of Newfoundland, St. John's, NL, A1B 3X5 Canada, e–mail: kazmy@mun.ca,

[b] Geological Museum, University of Copenhagen, Øster Voldgade 5, DK-1350 Copenhagen K, Denmark,

[c] Department of Earth Sciences, Brock University, St. Catharines, Ontario L2S 3A1 Canada,

[d] Dipartimento di Scienze della Terra, Universita` di Pisa, via Santa Maria 53, 56126 Pisa, Italy,

[e]1417 Fairbrook Dr., Des Peres, MO 63131, USA.

* Corresponding author: (e–mail: kazmy@mun.ca, Tel. 1 709 864 6731, Fax. 1 709 864 2589)

Abstract

The Green Point Formation of the Cow Head Group in western Newfoundland (Canada) represents the Global Stratotype Section and Point (GSSP) for the Cambrian–Ordovician boundary on Laurentia. The formation consists of the Martin Point (lower) and the Broom Point (upper) members, which constitute a thick (~170 m) deep subtidal to slope marine carbonate sequence. Preservation of the micritic carbonates of the Green Point Formation was evaluated by multiple petrographic and geochemical screening tools. The $\delta^{13}C$ and $\delta^{18}O$ values of near-primary micrites range from -4.7 ‰ to +1.7‰ (VPDB) and from -8.7 ‰ to -5.5 ‰ (VPDB), respectively, with no significant correlation ($R^2 = 0.002$). Similarly, the $\delta^{13}C$ values show no significant correlation with Mn/Sr ratios or total REE contents, which suggest that the investigated carbonates retain their near-primary $\delta^{13}C$ signatures that can be utilized to construct a high-resolution carbon-isotope profile for the GSSP. The $\delta^{13}C_{carb}$ profile about the GSSP trends generally positive into Bed 22 of the Green Point Formation. The top of the *C. intermedius* Zone marks the onset of a negative $\delta^{13}C_{carb}$ shift to about 6.0 ‰ culminating in the upper part of the zone. Subsequently, the $\delta^{13}C_{carb}$ profile trends positive with a 'double switch-back' about the boundary point and then continues on to a most positive value in the uppermost part of Bed 23. In addition, based on $^{87}Sr/^{86}Sr$ and Ce*/Ce values, the GSSP is defined by ratios of 0.709623 and <0.9, respectively, suggesting generally dysoxic waters before, during, and immediately after the boundary. The high-resolution chemostratigraphic results, curve, and trends covering the GSSP should facilitate correlation of the Cambrian–Ordovician boundary sections/sequences from other locations.

Key words: Cambrian–Ordovician GSSP, high-resolution $\delta^{13}C$ and $^{87}Sr/^{86}Sr$ chemostratigraphy, Green Point Formation

1. Introduction

Chemostratigraphy has great potential for refining the global stratigraphic correlations of sequences. Preserved primary/near-primary stable isotope signatures in marine carbonates, which are associated with time events, provide high-resolution profiles for correlating sedimentary sequences from different depositional settings and paleocontinents (e.g., Veizer et al., 1999; Halverson et al., 2005; Immenhauser et al., 2008, Azmy et al., 2010). Global sea-level changes along the eastern Laurentian margin about the Cambrian–Ordovician boundary influenced seawater redox condition, which was reflected in the carbon-isotopic composition of marine carbonates (e.g., Azmy et al., 2010). An informal C-isotope study of the Cambrian–Ordovician GSSP at Green Point (western Newfoundland, Canada), made about 20 years ago (Nowlan, 1995) is the only documentation of isotope compositions. This complicates correlating the GSSP with other sections with no useful biostratigraphic markers or ones complicated by depositional variations.

Since ratification of the GSSP at Green Point (Newfoundland, Canada), our understanding of C-isotope stratigraphy has greatly advanced, and modern techniques allow higher resolution and precision in analyses of not only the Green Point section, but also other boundary sections around the world. In this paper, we highlight the Cambrian–Ordovician GSSP at Green Point with high-resolution carbon and strontium isotope profiles supplemented by Ce* trends that allows for refining and enhancing the global correlation of the boundary interval.

2. Geologic Setting

Paleozoic sediments of western Newfoundland in Canada (Fig. 1) were deposited on the eastern Laurentian margin. The Laurentian plate developed by active rifting around 570 to 550 Ma (Cawood et al., 2001), and a pre–platform shelf formed and was eventually covered by clastic sediments (James *et al.* 1989). A major transgression flooded the Laurentian platform margin and resulted in the accumulation of thick carbonate deposits (Wilson et al., 1992; Lavoie et al., 2013). These platform deposits are dominated by high-energy carbonates that formed during the Middle and Late Cambrian, and were later buried under the low-energy carbonates of the St. George Group during the Early to earliest Middle Ordovician (cf. Knight et al., 2007, 2008; Lavoie et al., 2013).

3. Litho- and Biostratigraphy

The lithostratigraphy of the Cambrian–Ordovician boundary section, which is part of the Green Point Formation of the Cow Head Group (Fig. 2), has been studied and discussed in detail by James and Stevens (1986), and it will therefore be only summarized here. It consists of the uppermost Cambrian Martin Point and lowermost Ordovician Broom Point members, which are generally composed of dark grey to black fissile shale alternating with thin (~ 1 cm-thick) interbeds of ribbon limestone rhythmites. Siltstone interbeds (up to 1 cm thick) may co-occur with shale, and the limestone interbeds vary from isolated and thin to up to 20 cm thick. The conglomerate beds contain blocks of shallow water carbonates that were transported into deep-water facies along the slope of the Laurentian margin (James and Stevens, 1986).

The Cambrian–Ordovician GSSP section at Green Point spans the *Cordylodus intermedius* (Furongian, uppermost Cambrian) to the *Cordylodus angulatus* Zones (Tremadocian, Lower Ordovician) and is defined by the FAD of the conodont *Iapetognathus fluctivagus* (Figs. 2 and 3;

Cooper et al., 2001). The current spike marking the Cambrian–Ordovician boundary in the GSSP section at Green Point (Fig. 2) is placed within Bed 23 (Cooper et al., 2001). Sometimes stratigraphic boundaries and sequences including GSSPs are difficult to correlate with others due to a lack of fossils (Cooper et al., 2001; Terfelt et al., 2012, Fig. 3), which makes carbon isotope chemostratigraphy a valuable and important tool for GSSPs and their global correlation.

4. Methodology

Eighty two samples (Appendix 1, Fig. 2) were collected at high resolution (sampling intervals as small as 10 cm) from the Cambrian–Ordovician GSSP boundary section (49° 40′ 51″ N; 57° 57′ 36″ W) at Green Point, western Newfoundland (Fig. 1). Samples were taken from laminated lime mudstone rhythmites to avoid allochthonous clasts. Thin sections of samples were petrographically examined with a polarizing microscope and stained with Alizarin Red–S and potassium ferricyanide solutions (Dickson, 1966). Cathodoluminescence (CL) observations were performed using a Technosyn 8200 MKII cold cathode instrument operated at 8 kV accelerating voltage and 0.7 mA current.

A mirror-image slab of each thin section was also prepared and polished for microsampling. These polished slabs were washed with deionized water and dried overnight at 50 ^{o}C prior to isolating the finest grained lime mudstone free of secondary cements and other contaminants. Approximately, 10 mg of carbonate were microsampled from the cleaned slabs using a low-speed microdrill under binocular microscope.

For C- and O-isotope analyses, about 220 μg of powder sample was reacted in an inert atmosphere with ultrapure concentrated (100 %) orthophosphoric acid at 70 ^{o}C in a Thermo–Finnigan GasBench II. The liberated CO_2 was automatically delivered to a ThermoFinnigan

DELTA V plus isotope ratio mass spectrometer in a stream of helium, where the gas was ionized and measured for isotope ratios. Uncertainties of better than 0.1‰ (2σ) for the analyses were determined by repeated measurements of NBS–19 ($\delta^{18}O$ = –2.20‰ and $\delta^{13}C$ = +1.95‰ vs. VPDB) and L–SVECS ($\delta^{18}O$ = –26.64 ‰ and $\delta^{13}C$ = –46.48 ‰ vs. VPDB). Our dataset has been complemented by the unpublished results obtained and mentioned in the task group report of Nowlan (1995).

A subset of representative samples was selected for Sr-isotope analysis. About 3 mg of the powdered sample was dissolved in 2.5 N ultrapure HCl and after evaporation Sr was extracted with quartz glass exchange columns filled with Bio Rad AG50WX8 ion exchange resin. About 100 µg Sr was loaded on Re filaments using a Ta_2O_5-HNO_3-HF-H_3PO_4 solution. Measurements were performed with a Finnigan MAT 262 multicollector mass spectrometer at the Institut für Geologie, Mineralogie und Geophysik, Ruhr Universität, Bochum, Germany (cf. Azmy et al., 1999, 2001).

Two standard reference materials were utilized for quality control of Sr isotope ratio measurements, NIST (NBS) 987 and USGS EN-1. The latter, representing modern seawater and treated like an ordinary sample, gave a $^{87}Sr/^{86}Sr$ value of 0.709170±0.000008 (2σ calculated from 17 measurements). About 75 µg Sr of the NIST (NBS) 987 standard reference material was directly loaded onto the filament and these results therefore represent only the internal reproducibility of mass-spectrometry. Its value was 0.710246±0.000008, based on 29 measurements. The average composite blank for Sr, including chemicals, ion-exchange columns and loading blank, did not exceed 0.0085 µg. The measured $^{87}Sr/^{86}Sr$ ratio was normalized to a value of 8.375209 for the $^{88}Sr/^{86}Sr$ ratio. All $^{87}Sr/^{86}Sr$ measurements were normalized to the NBS 987 value of 0.710247 (McArthur, 1994).

137 For elemental analyses, a subset of sample powder was digested in 5 % (v/v) acetic acid for
138 70–80 min. and analysed for major, minor and rare earth elements (REE) using an Elan DRC II
139 ICP-MS (Perkin Elmer SCIEX) at Memorial University of Newfoundland. The relative
140 uncertainties of these measurements are less than 5 %, and results are normalized to a 100 %
141 carbonate basis (cf. Brand and Veizer, 1980).
142
143 **5. Results**
144 Petrographic investigation shows that the sampled carbonates are dominantly rhythmites,
145 which have retained their near-micritic texture (Fig. 4a-b). They appear dull to non-luminescent
146 under cathodoluminoscence. Phosphatic algae occur as embedded aggregates and/or laminae
147 (Fig. 4c-d) in the topmost carbonate bed of the Martin Point Member (Fig. 2, Bed 22) that
148 otherwise consists of peloidal - algal grainstones.
149 The geochemical attributes of the investigated carbonates are presented in detail in Appendix
150 1. The Sr and Mn values are poorly correlated (R^2=0.08) and similarly the Mn/Sr ratios with
151 the $\delta^{13}C_{carb}$ values (R^2=0.06). The $\delta^{13}C_{carb}$ values show no correlation with their $\delta^{18}O_{carb}$
152 counterparts (R^2=0.002). Although $\delta^{13}C_{carb}$ values exhibit poor correlation with their total REE
153 (∑REE) contents, the $\delta^{18}O_{carb}$ values show in contrast a significant correlation with ∑REE
154 contents (Fig. 5a). Also, the $^{87}Sr/^{86}Sr$ values exhibit poor correlation with their 1/Sr counterparts
155 (Fig. 5b). The Ce*/Ce (Ce-anomaly indicator) values exhibit narrow variations between 0.8 and
156 1 below and immediately above the boundary (Fig. 6).
157 **6. Discussion**
158 Carbon-isotope chemostratigraphy is mainly based on the distinctive variations in the $\delta^{13}C_{carb}$
159 profile of the investigated sequence. These variations may reflect environmental and/or

diagenetic perturbations (Appendix 1, Fig. 6). It is almost impossible, particularly for ancient sediment, to stay entirely unaffected by diagenetic fluids through geologic time. However, it is possible that alteration was so limited that allowed carbonates to retain, at times, near-primary signatures. Therefore, evaluation and proof of retained (primary or near-primary) isotopic and elemental geochemical signatures is a cornerstone for the reconstruction of high-resolution chemostratigraphic profiles important for global correlation.

6.1 Evaluation of Sample Preservation

The Green Point Formation at the GSSP spans the Cambrian–Ordovician boundary and is dominated by lime mudstone rhythmites that show insignificant recrystallization (Fig. 4a). They retained original sedimentary fabrics and a micritic to near-micritic grain size, thus suggesting a high degree of textural preservation. They also exhibit non- to dull luminescence under cathodoluminoscope (Fig. 4b). Luminescence in carbonates is mainly activated by high concentrations of Mn and quenched by high concentrations of Fe (Machel and Burton, 1991). Dull luminescence, in many cases, indicates relative preservation of primary geochemical signatures although altered carbonates might still exhibit no luminescence due to high Fe contents (Rush and Chafetz 1990) and cathodoluminescence is, therefore, a single evaluation tool that has to be complemented additional tests (Brand et al., 2011).

Diagenesis results mainly in depletion in Sr and $\delta^{18}O$ values but enrichment in Mn and ∑REE counterparts (Brand and Veizer, 1980; Veizer, 1983; Azmy et al., 2011). Therefore, the Mn/Sr values of marine carbonates, when correlated with their $\delta^{13}C$ and $\delta^{18}O$ counterparts, can be utilized for evaluating the degree of preservation (e.g., Derry et al., 1992; Kaufman and Knoll, 1995). The Mn/Sr values of the investigated lime mudstones are insignificantly correlated with

183 their $\delta^{13}C$ counterparts (R^2=0.06), suggesting preservation of near-primary $\delta^{13}C$ values. ∑REE
184 contents of carbonates are sensitive, like $\delta^{18}O$, to the slightest of alteration and are significantly
185 enriched by diagenesis, and have been proven a powerful tool in recognizing alteration in
186 carbonates (e.g., Azmy et al., 2011, 2012). Despite a considerable correlation between the ∑REE
187 and $\delta^{18}O$ values (Fig. 5a) due to minor alterations, the correlation of ∑REE with $\delta^{13}C$ is
188 insignificant (Fig. 5b), thus supporting preservation of primary/near-primary $\delta^{13}C$ signatures of
189 the Green Point carbonates. On the other hand, the previously implied involvement of light ^{12}C
190 from immediate post-depositional diagenesis of organic matter (Nowlan, 1995) would not
191 consistently deplete the $\delta^{13}C$ of the carbonates only in the upper part of the section, where the
192 negative $\delta^{13}C$ excursion occurs, without causing the same effect in the lower part particularly
193 when organic-rich shale interbeds occur throughout the sequence. In addition, the GSSP
194 carbonates were deposited in deep shelf to slope settings (James and Stevens, 1986) under
195 oxygen-poor conditions, which makes a contribution of ^{12}C from the oxidation of organic matter
196 unlikely. Therefore, our screening evaluation suggests that the $\delta^{13}C$ signatures of the investigated
197 carbonates are reliable and robust and can be utilized to reconstruct a high-resolution C-isotope
198 profile for the Cambrian−Ordovician GSSP.
199 The $^{87}Sr/^{86}Sr$ values show insignificant correlation with their 1/Sr counterparts (R^2 =0.2),
200 which supports preservation of near-primary Sr-isotope signatures (Fig. 5b).
201 Variations in sealevel, particularly those associated with time events, are generally associated
202 with changes in trace and rare earth elements concentrations in sediments due to inputs of
203 terrestrial material and changes in redox conditions (e.g., Wignall and Twitchett, 1996; Murphy
204 et al., 2000; Arnaboldi and Meyers, 2007; Wignall et al., 2007; Piper and Calvert, 2009;
205 Śliwiński et al., 2010). Therefore, major $\delta^{13}C$ shifts of time events reflect relative changes in

organic productivity and paleoredox. However, the section at Green point consists of carbonates deposited in a slope setting generally well below the photic zone (James and Stevens, 1986) where biota abundance is low. The occurrence of phosphatic laminated algae or aggregates (Fig. 4c) explains the phosphorous spike immediately below the negative $\delta^{13}C$ excursion (Fig. 6), which is also consistent with the correlated high ∑REE value (Fig. 6).

Levels of oxygen in the water column influence the oxidation state of some elements and selectively control their solubility in seawater and consequently their enrichment in marine sediments (e.g., Wignall and Twitchett, 1996; Arnaboldi and Meyers, 2007, Wignall et al., 2007). Despite diagenetic alteration, Ce/Ce* values in ancient micritic/near-micritic sediments have been found insignificantly affected by diagenesis and may provide a proxy of the redox condition of seawater (e.g., Loope et al., 2013). Most of the Ce/Ce* values of the GSSP carbonates range from 0.75 to 0.97 (Fig. 6), which suggests dysoxic conditions for the deep shelf to slope setting sediments (de Baar et al., 1988; German and Elderfield, 1990; Bau and Dulski, 1996); an interpretation reconcilable with the occurrence of the phosphatic algae.

6.2 Carbon-isotope Stratigraphy

Accepting that the Green Point carbonates retained at least their near-primary $\delta^{13}C$ signatures, a reliable stratigraphic C-isotope profile can be reconstructed to investigate temporal variations in seawater chemistry around the Cambrian–Ordovician boundary.

The $\delta^{13}C$ profile of Green Point Formation (Fig. 6) shows no significant variations until near the boundary between the Martin Point and Broom Point members near the top of Bed 22 when a composite negative shift, consisting of 5 peaks and extending into the lower part of Bed 26, starts

with a sharp swing of about 6 ‰ (Fig. 6). No physical stratigraphic hiatuses have been documented at this shift (cf. James and Stevens, 1986; Cooper et al., 2001; Terfelt et al., 2012).

At the transition from the Cambrian to the Ordovician, the $\delta^{13}C$ curve changes from a negative excursion (~ -5 ‰) to a positive one (~ +2 ‰) accentuated by a 'double switch-back right about the boundary (inset Fig. 6). These unique features – the negative to positive shift interrupted by the double switch-back – should be important features in delineating and refining the boundary position in other sequences at other locations.

Similar but small shifts, between 2.5 and <1 ‰, have been documented in the C-isotope profiles of other boundary sections from different localities and were correlated with stratigraphic levels correlated with the *intermedius* or the *intermedius / lindstromi* boundary such as in the Black Mountain Australia (Ripperdan et al., 1992, their Fig. 1), Xiaoyanqiao near Diangcha (Jilin Province, China, Ripperdan et al., 1993, their Fig. 2), Lawson Cove (Utah, USA, Nowlan, 1995; his Figs. 1 and 2), Kazakhestan (Nowlan,1995; his Fig. 2), Argentine (Buggish et al., 2003), and China (e.g., Kalpin region of Tarim Basin, Jing et al., 2006, their Fig. 5). The magnitude of a $\delta^{13}C$ excursion on an isotope profile relies mainly on the response of organic primary productivity (OPP) that varies from environment to another and also from basin to basin particularly when dealing with carbonate rhythmites of deep shelf to slope settings in the Green Point section where drop in organic productivity, associated with possible relative sealevel rise (Fig. 2), at that depth is expected to enhance the negative $\delta^{13}C$ excursion on the isotope profile. However, it is beyond the scope of the current investigation to evaluate the $\delta^{13}C$ curves documented in other global sections (e.g., Ripperdan et al., 1993; Jing et al., 2006).

Negative $\delta^{13}C$ excursions of comparable values (4 to 8 ‰) to that of the GSSP profile (~ 6 ‰), and caused by variations in primary productivity, have been documented in carbonates of

similar environments from the Precambrian (e.g., Azmy et al., 2001, 2006; Halverson et al., 2005) and Paleozoic (e.g., Azmy et al., 2012).

6.3 Sr-isotope variations around the boundary

The Sr-isotope profile shows a considerable inflection point correlated with the starting point of the composite negative $\delta^{13}C$ shift (Fig. 6) and also with minimum values on the ∑REE profile, which confirms the preservation of near-primary $^{87}Sr/^{86}Sr$ signatures. The $^{87}Sr/^{86}Sr$ values at the Green Point GSSP boundary section (Fig. 6) fall within the documented range of its global counterparts and comparable inflection points have been reported from other boundary sections on different paleocontinents (Veizer et al., 1999; Ebneth et al., 2001). Low-resolution field sampling (wide sampling intervals) of those sections (e.g., Ebneth et al., 2001) is most likely the cause of missing the strong inflection point (0.710852, Appendix 1) recorded by the Green Point GSSP Sr-isotope profile around the boundary (inset Fig. 6).

7. Conclusions

Samples were collected at high-resolution from the lime mudstone beds (rhythmites) of the Cambrian–Ordovician GSSP boundary section at Green Point in western Newfoundland, Canada. Petrographic and geochemical screening suggests preservation of near-primary $\delta^{13}C$ signatures.

The $\delta^{13}C$ profile exhibits a negative excursion that starts at a stratigraphic level near the middle of Bed 22, slightly below the boundary between the Martin Point and Broom Point members and about 2 m below the Cambrian–Ordovician boundary. A positive shift from ~ -5 ‰

to ~ 2‰ coupled with a double switch-back about the boundary are unique features at the GSSP that should aid in the correlation of other Cambrian–Ordovician boundary sections.

The $^{87}Sr/^{86}Sr$ profile spanning the lower part of the $\delta^{13}C$ excursion shows a spike correlated with low ∑REE, which supports preservation of primary Sr-isotope signatures and the spike corresponds with the negative $\delta^{13}C$ excursion at the Green Point GSSP.

The stratigraphic level of the start of negative $\delta^{13}C$ excursion and the associated $^{87}Sr/^{86}Sr$ spike suggest a chemostratigraphic anomaly that can be utilized for correlattion with other global sections spanning the Cambrian–Ordovician boundary.

The difference in the stratigraphic level between the golden spike, which marks the current Cb–O boundary based on conodont biostratigraphy, and the underlying geochemical anomaly is likely attributed to the lag time between the geochemical oceanographic changes and the response of marine biota particularly in the deep shelf and slope settings.

Acknowledgements

The authors wish to thank Drs. ….. and …….. for their constructive reviews. Also, the efforts of Drs. …….. (editor) and …….. (Journal manager) are much appreciated. This project was supported by funding (to Karem Azmy) from Petroleum Exploration Enhancement Program (PEEP) and (to Svend Stouge) from the Danish Research Council.

References

Arnaboldi, M., Meyers, P.A., 2007. Trace element indicators of increased primary production and decreased water-column ventilation during deposition of latest Pliocene sapropels at five locations across the Mediterranean Sea. Palaeogeography, Palaeoclimatology, Palaeoecology 249, 425–443.

297 Azmy, K., Brand, U., Sylvester, P., Gleeson, S., Logan, A., Bitner, M.A., 2011. Biogenic low–
298 Mg calcite (brachiopods): proxy of seawater–REE composition, natural processes and diagenetic
299 alteration. Chemical Geology 280, 180-190.

300 Azmy, K., Kaufman, A.J., Misi, A., Oliveira, T.F., 2006. Isotope stratigraphy of the Lapa
301 Formation, São Francisco Basin, Brazil: Implications for Late Neoproterozoic glacial events in
302 South America. Precambrian Research 149, 231–248.

303 Azmy, K., Lavoie, D., 2009. High–resolution isotope stratigraphy of the Lower Ordovician St.
304 George Group of western Newfoundland, Canada: implications for global correlation. Canadian
305 Journal of Earth Sciences 46, 1–21.

306 Azmy, K., Mottequin, B., Poty, E., 2012. Frasnian-Famenian pre-event: a record from the Dinant
307 Basin, Belgium. Palaeogeography, Palaeoclimatology, Palaeoecology 313, 93-106.

308 Azmy, K., Stouge, S., Christiansen, J.L., Harper, D.A.T., Knight, I., Boyce, D., 2010. Carbon-
309 isotope stratigraphy of the Lower Ordovician succession in Northeast Greenland: implications
310 for correlations with St. George Group in western Newfoundland (Canada) and beyond.
311 Sedimentary Geology 225, 67-81.

312 Azmy, K., Veizer, J., Misi, R., De Olivia, T., Sanches, A.L., Dardenne, M., 2001. Isotope
313 Stratigraphy of the Neoproterozoic Carbonate of Vazante Formation Saõ Francisco Basin, Brazil.
314 Precambrian Research 112, 303–329.

315 Azmy, K., Veizer, J., Wenzel, B., Bassett, M. and Copper, P., 1999. Silurian strontium isotope
316 stratigraphy. Geological Society of America Bulletin, 111, 475-483.

317 Banner, J.L., Hanson, G.N., 1990. Calculations of simultaneous isotopic and trace element
318 variations during water–rock interaction with applications to carbonate diagenesis. Geochimica
319 et Cosmochimica Acta 54, 3123–3137.

320 Bau, M., Dulski, P., 1996. Distribution of yttrium and rare-earth elements in the Penge and
321 Kuruman iron-formations, Transvaal Supergroup, South Africa. Precambrian Research 79, 37-
322 55.
323 Brand, U., Veizer, J., 1980. Chemical diagenesis of a multicomponent carbonate system: 1.
324 Trace elements. Journal of Sedimentary Petrology 50, 1219–1236.

325 Buggisch, W., Keller, M., Lehnert, O., 2003. Carbon isotope record of Late Cambrian to Early
326 Ordovician carbonates of the Argentine Precordillera. Palaeogeography, Palaeoclimatology,
327 Palaeoecology 195, 357-373.
328 Cawood, P.A., McCausland, P.J.A., Dunning, G.R., 2001. Opening Iapetus: Constraints from
329 Laurentian margin in Newfoundland. Geological Society of America Bulletin 113, 443–453.

330 Cooper, R.A., Nowlan, G.S., Williams, S.H., 2001. Global Stratotype Section and Point for base
331 of the Ordovician System. Episodes 24, 19–28.

de Baar, H.J.W., German, C.R., Elderfield, H., van Gaans, P., 1988. Rare earth element distributions in anoxic waters of the Cariaco Trench. Geochimica et Cosmochimica. Acta 52, 1203–1219.

Derry, L.A., Kaufman, A.J., Jacobsen, S.B., 1992. Sedimentary cycles and environmental change in the Late Proterozoic: evidence from stable and radiogenic isotopes. Geochimica et Cosmochimica Acta 56, 1317–1329.

Dickson, J.A.D., 1966. Carbonate identification and genesis as revealed by staining. Journal of Sedimentary Petrology 36, 491–505.

Ebneth, S., Shields, G.A., Veizer, J., Miller, J.F., Shergold, J.H., 2001. High-resolution strontium isotope stratigraphy across the Cambrian-Ordovician transition. Geochimica et Cosmochimica Acta 65, 2273–2292.

German, C.R., Elderfield, H., 1990. Application of the Ce anomaly as a paleoredox indicator: the ground rules. Paleocean 5, 823–833.

Halverson, G.P., Hoffman, P.F., Schrag, D.P., Maloof, A.C., Rice, A.H.N., 2005. Toward a Neoproterozoic composite carbon–isotope record. Geological Society of America Bulletin 117, 1181–1207.

Immenhauser, I., Holmden, C., Patterson, W.P., 2008. Interpreting the carbon–isotope record of ancient shallow epiric seas: lessons from the Recent. In: Pratt B.R., Holmden, C. (Eds.), Dynamics of epeiric seas, Geological Association of Canada, Special Paper 48, 137–174.

James, N.P., Stevens, P.K., 1986. Stratigraphy and correlation of the Cambro–Ordovician Cow Head Group, western Newfoundland. Geological Survey of Canada Bulletin 366, 1–143.

James, N.P., Stevens, R.K., Barnes, C.R., Knight, I., 1989. Evolution of a Lower Paleozoic continental–margin carbonate platform, northern Canadian Appalachians In: Crevello, P. D. Wilson, J. L. Sarg, J. F. Read, J. F. (Eds.), Controls on Carbonate Platform and Basin Development, Society of Economic Paleontologists and Mineralogists Special Publication 44, 123–146.

Jing, X-C, Deng, S-H, Zhao, Z-J, Lu, Y-Z, Zhang, S-B, 2008. Carbon isotope composition and correlation across the Cambrian-Ordovician boundary in Kalpin Region of the Tarim Basin, China. Science in China: Earth Sciences 51, 1317-1359.

Kaufman, A.J., Knoll, A.H., 1995. Neoproterozic variations in the C–isotopic composition of seawater: stratigraphic and biogeochemical implications. Precambrian Research 73, 27–49.

Knight, I., Azmy, K., Boyce, D., Lavoie, D., 2008. Tremadocian carbonates of the lower St. George Group, Port au Port Peninsula, western Newfoundland: Lithostratigraphic setting of diagenetic, isotopic, and geochemistry studies. Current Research Newfoundland and Labrador Department of Natural Resources Geological Survey. Report 08–1, 1–43.

Knight, I., Azmy, K., Greene, M., Lavoie, D., 2007. Lithostratigraphic setting of diagenetic, isotopic, and geochemistry studies of Ibexian and Whiterockian carbonates of the St. George and Table Head groups in western Newfoundland. Current Research Newfoundland and Labrador Department of Natural Resources Geological Survey. Report 07–1, 55–84.

Lavoie, D., Desrochers, A., Dix, G., Knight, A. Hersi, O.S., 2013. The great carbonate Bank in eastern Canada: an overview. In: Derby, J., Fritz, R., Longcare, S., Morgan, W., Sternbach, C., (Eds.), The Great American Carbonate Bank: the Geology and Economic Resources of Cambrian−Ordovician Sauk Megasequence of Laurentia. American Association of Petroleum Geologists, Memoir 98, 499–524.

Lécuyer, C., Grandjean, P., Barrat, J.-A., Nolvak, J., Emig, C., Paris, F., Robardet, M., 1998. $\delta^{18}O$ and REE contents of phosphatic brachiopods: a comparison between modern and lower Paleozoic populations. Geochimica et Cosmochimica Acta 62, 2429–2436.

Loope, G.R., Kump, L.R., Arthur, M.A. 2013. Shallow water redox conditions from the Permian–Triassic boundary microbialite: the rare earth element and iodine geochemistry of carbonates from Turkey and South China. Chemical Geology 351, 195–208.

Machel, H.G., Burton, E.A., 1991. Factors governing cathodoluminescence in calcite and dolomite, and their implications for studies of carbonate diagenesis. In: Luminescence microscopy and spectroscopy, qualitative and quantitative applications, SEPM Short Course 25, 37–57.

McArthur, J.M., 1994. Recent trends in strontium isotope stratigraphy. Terra Nova 6, 331–358.

Morel, F.M.M., Milligan, A.J., Saito, M.A., 2004. Marine bioinorganic chemistry: the role of trace metals in the oceanic cycles of major nutrients. In: Elderfield, H., Holland, H.D., Turekian, K.K. (Eds.), The Oceans and Marine Geochemistry, Treatise on geochemistry, volume 6. Elsevier, Amsterdam, Heidelberg, pp. 113–143.

Murphy, A.E., Sageman, B.B., Hollander, D.J., Lyons, D.J., Brett, C.E., 2000. Black shale deposition and faunal overturn in the Devonian Appalachian basin: Clastic starvation, seasonal water column mixing, and efficient biolimiting nutrient recycling. Paleoceanography 15, 280-291.

Mussman, W.J., Read, J.G., 1986. Sedimentology and development of a passive margin unconformity: Middle Ordovician Knox Unconformity, Virginia Appalachians. Bulletin of Geological Society of America 97, 282–295.

Nowlan, G.S., 1995 (unpublished). Variations in marine carbon isotope ratios ($\delta^{13}C$) through the Cambrian-Ordovician boundary interval. International Cambrian-Ordovician boundary working group. St. John's, Newfoundland (Canada), December, 1995.

Piper, D.Z., Calvert, S.E., 2009. A marine biogeochemical perspective on black shale deposition. Earth-Science Reviews 95, 63–96.

402 Ripperdan, R.L., Magaritz, M., Kirschvink, J.L., 1993. Carbon isotope and magnetic polarity
403 evidence for non-depositional events within the Cambrian-Ordovician boundary section at
404 Dayangcha. Jilin Province, China. Geological Magazine 130, 443-452.

405 Ripperdan, R.L., Magaritz, M., Nicoll, R.S., Shergold, J.H., 1992. Simultaneous changes in
406 carbon isotopes, sealevel, and conodont biozones within the Cambrian-Ordovician boundary
407 interval at Black Mountain, Australia. Geology 20, 1039-1042.

408 Rush, P.F., Chafetz, H.S., 1990. Fabric retentive, non–luminescent brachiopods as indicators of
409 original $\delta^{13}C$ and $\delta^{18}O$ compositions: a test. Journal of Sedimentary Petrology 60, 968–981.

410 Scotese, C. R., 2 002. PALEOMAP Project. http://www.scotese.com

411 Śliwiński, M.G., Whalen, M.T., Day, J., 2010. Trace element variations in the Middle Frasnian
412 punctata zone (Late Devonian) in the western Canada sedimentary Basin–changes in oceanic
413 bioproductivity and paleoredox spurred by a pulse of terrestrial afforestation? Geologica Belgica
414 4, 459–482.

415 Stenzel, S.R., Knight, I., James, N.P., 1990. Carbonate platform to foreland basin: revised
416 stratigraphy of the Table Head Group (Middle Ordovician), western Newfoundland. Canadian
417 Journal of Earth Sciences 27, 14–26.

418 Terfelt, F., Bagnoli, G., Stouge, S., 2102. Re-evaluation of the conodont *Iapetognathus* and
419 implications for the base of the Ordovician System GSSP. Lethaia 45, 227–237.

420 Veizer, J. 1983. Chemical diagenesis of carbonates. In: Arthur, M.A., Anderson, T.F., Kaplan, I.
421 R., Veizer, J., Land, L.S. (Eds.), Theory and application of trace element technique, Stable
422 Isotopes in Sedimentary Geology. Society of Economic Paleontologists and Mineralogists
423 (SEPM) Short Course Notes 10, III–1–III–100.

424 Veizer, J., Ala, D., Azmy, K.; Bruckschen, P., Bruhn, F, Buhl, D. Carden, G., Diener, A.,
425 Ebneth, S., Goddris, Y., Jasper, T., Korte, C., Pawellek, F., Podlaha, O., Strauss, H., 1999.
426 $^{87}Sr/^{86}Sr$, $\delta^{18}O$ and $\delta^{13}C$ evolution of Phanerozoic seawater. Chemical Geology 161, 59–88.

427 Wignall, P.B., Twitchett, R.J., 1996. Oceanic anoxia and the end Permian mass extinction.
428 Science 272, 1155–1158.

429 Wignall, P.B., Zonneveld, J.-P., Newton, R.J., Amor, K., Sephton, M.A., Hartley, S., 2007. The
430 end Triassic mass extinction record of Williston Lake, British Columbia, Palaeogeography,
431 Palaeoclimatology, Palaeoecology 253, 385–406.

432 Wilson, J.L., Medlock, P.L., Fritz, R.D., Canter, K.L., Geesaman, R.G., 1992. A review of
433 Cambro–Ordovician breccias in North America, *in*: M. P. Candelaria and C. L. Reed, eds.,
434 Paleokarst, karst–related diagenesis and reservoir development. SEPM–Permian Basin Section,
435 Publication 92–33, 19–29.

436

LIST OF FIGURES

Fig. 1. Location map of Green Point, western Newfoundland, Canada showing (A) the location of the GSSP Cambrian-Ordovician boundary section in eastern Canada, (B) the distribution of outcrops of the beds covering the boundary interval (modified from Cooper et al., 2001), and global (C) boundary sections (based on Scotese, C. R., 2002, PALEOMAP Project, http://www.scotese.com) from Lawson Cove (Utah, USA), Llano (Texas, USA), Batyrbai Range (Kazakhstan), Wushi (S. China), Kalpin (S. China), Black Mountain (Australia), and Dayangcha, Jilin (N. China).

Fig. 2. Stratigraphic framework of the investigated Cambrian–Ordovician GSSP boundary section in western Newfoundland, Canada showing the detailed measured section with the positions of investigated samples and conodont zonation scheme (modified from Cooper et al., 2001).

Fig. 3. Correlation of conodont biozones for the Cambrian-Ordovician interval on the Larentian platform with North and South China (after Terfelt et al., 2012).

Fig. 4. Photomicrographs of the investigated carbonates showing, (a) micritic lime mudstones (Sample GP 21), (b) CL image of (a), (c) embedded phosphatic algae (arrows, Sample GP 28) in peloidal to algal grainstones, and (d) CL image of (c) where the phosphatic algae appear non-CL compared to the whole rock that exhibit dull CL.

Fig. 5. Scatter diagrams showing correlations of (a) ∑REE vs. $\delta^{13}C$ and $\delta^{18}O$, and (b) 1/Sr vs. $^{87}Sr/^{86}Sr$ for the micritic lime mudstones from the investigated sequence.

Fig. 6. Carbon- and Sr-isotopes, P, ∑REE, and Ce/Ce* profiles showing variations across the Cambrian–Ordovician GSSP boundary in Green Point (western Newfoundland, Canada). The Ce anomaly [$(Ce/Ce^*)_{SN} = Ce_{SN}/(0.5La_{SN}+0.5Pr_{SN})$] was calculated with the equations of Bau and

Dulski (1996). The grey dots trace the earlier profile reconstructed from Nowlan (1995) and the solid grey line refers to the level of the geochemical anomaly recorded in the current study, which is correlated with the FAD of the *C. intermedius* (i.e. at the top of Bed 22). The dashed black line marks the current position of the Cambrian−Ordovician boundary based on FAD of *I. flactivagus* (Cooper et al., 2001). The empty circles (red) are the complementary data by Ripperdan that were mentioned in the report of Nowlan (1995). The inset is a close-up of variations in the $\delta^{13}C$ and $^{87}Sr/^{86}Sr$ profiles from Beds 21 to 24 spanning the stratigraphic level of the geochemical anomaly (in Bed 22) and the current Cambrian–Ordovician biostratigraphic boundary (Bed 23). Legend as in Fig. 2.

Appendix 1. Elemental and isotopic geochemical compositions of Green Point carbonates. Concentrations of elements are in ppm and all values proceeded by the sign "<" are below the detection limit.

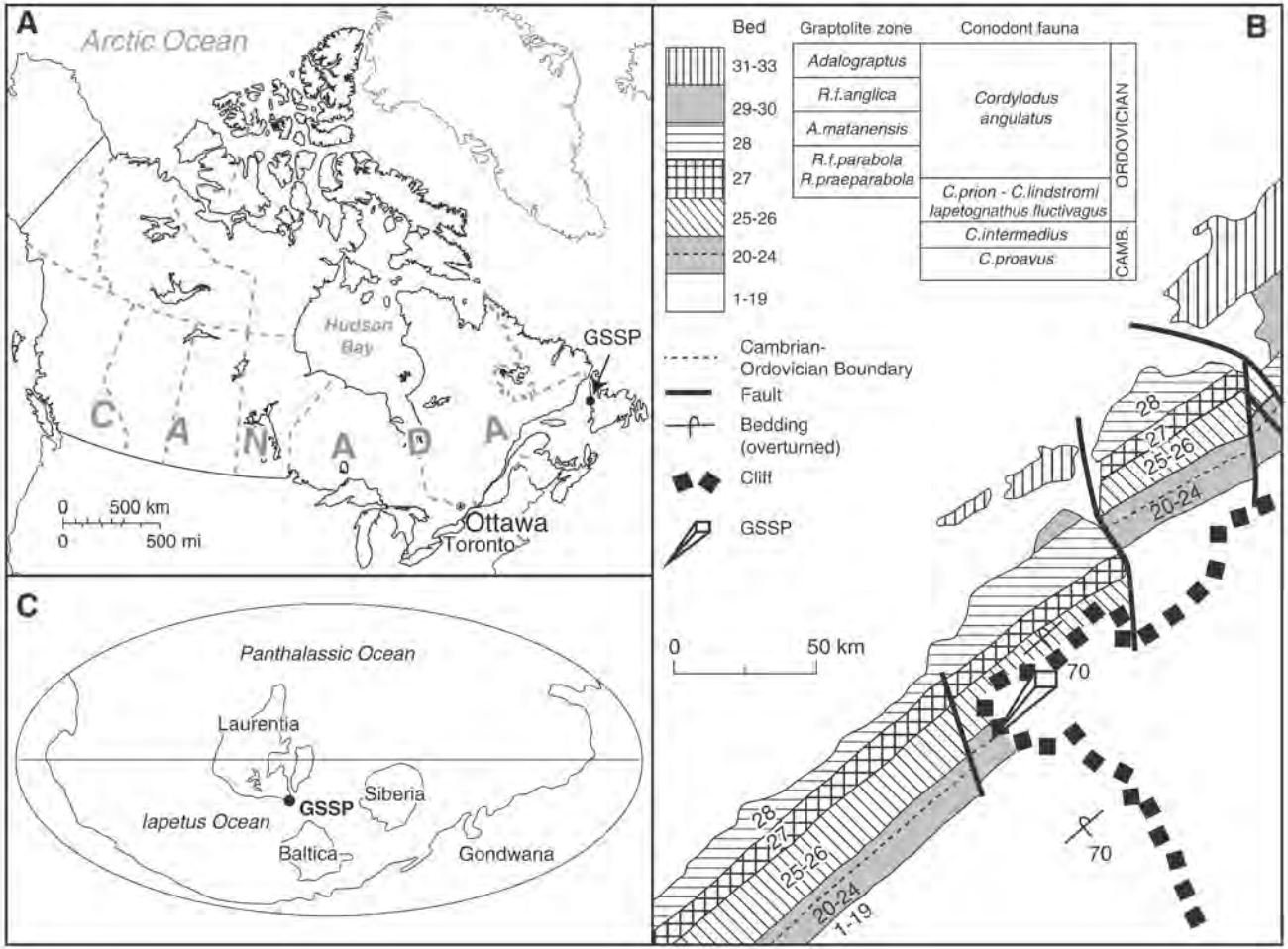
A
Arctic Ocean
Hudson Bay
GSSP
C A N A D A
0 500 km
0 500 mi
Ottawa
Toronto
B
Bed
Graptolite zone
Conodont fauna
31-33
29-30
28
27
25-26
20-24
1-19
Adalograptus
R.f.anglica
A.matanensis
R.f.parabola
R.praeparabola
Cordylodus angulatus
C.prion - C.lindstromi
Iapetognathus fluctivagus
C.intermedius
C.proavus
ORDOVICIAN
CAMB.
Cambrian-Ordovician Boundary
Fault
Bedding (overturned)
Cliff
GSSP
0 50 km
70
C
Panthalassic Ocean
Laurentia
Siberia
GSSP
Iapetus Ocean
Baltica
Gondwana

Fig. 1.

CAMBRIAN
ORDOVICIAN
Furongian
Tremadocian
Cow Head Group
Green Point Formation
Broom Point Member
Martin Point Member
17
18
19
20
21
22
23
24
25
26
27
28
m
sh
si
md
gn
cg
GP 82
GP 81
GP 80
GP 79
GP 78
GP 77
GP 76
GP 75
GP 74
GP 73
GP 72
GP 71
GP 70
GP 69
GP 68
GP 67
GP 66
GP 65
GP 64
GP 63
GP 62
GP 61
GP 60
GP 59
GP 58
GP 57
GP 56
GP 55
GP 54
GP 53
GP 52
GP 51
GP 50
GP 49
GP 48
GP 47
GP 46
GP 45
GP 44
GP 43
GP 42
GP 41A
GP 41
GP 40A
GP 40
GP 39
GP 38
GP 37
GP 36
GP 35
GP 34
GP 33A
GP 33
GP 31
GP 30
GP 32
GP 27-29
GP 26
GP 25
GP 24
GP 23
GP 22
GP 21
GP 20
GP 19
GP 18
GP 17
GP 16
GP 15
GP 14
GP 13
GP 12
GP 11
GP 10
GP 9
GP 8
GP 7
GP 6
GP 5
GP 4
GP 3
GP 2
GP 1
Cordylodus proavus
C.int
I. fluctivagus
Cordylodus angulatus
shale
siltstone
limestone
Breccia/ conglomerate
md mudstone
gn grainstone
nodules
graptolite
crossbedding
Cb-O boundary (Golden spike)

Fig. 2.

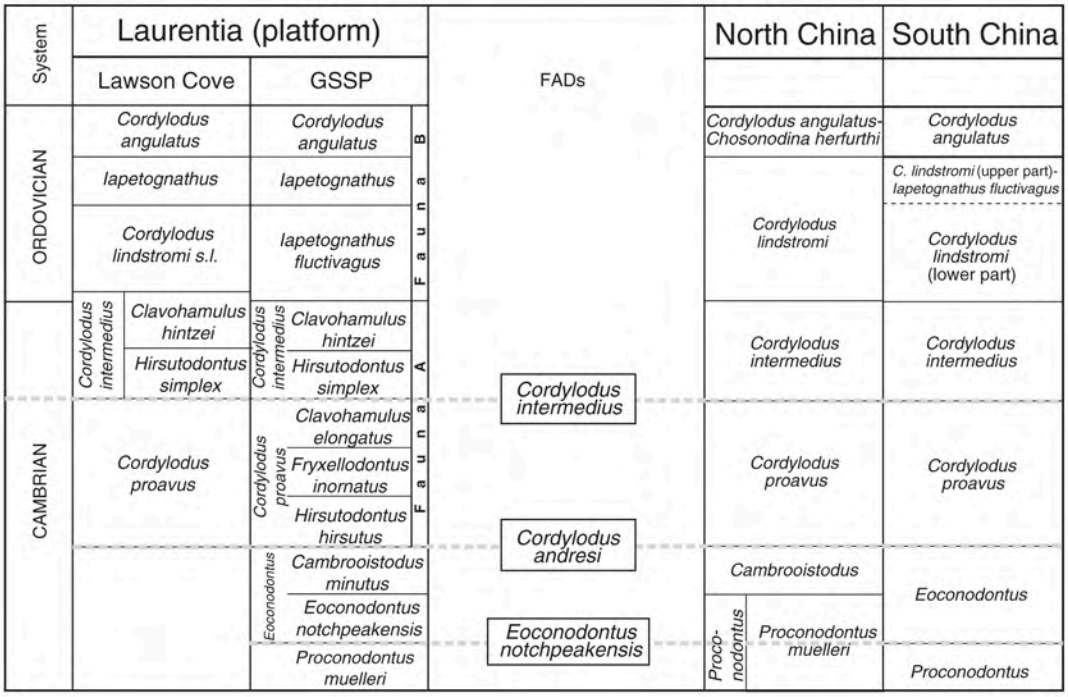
System
Laurentia (platform)
Lawson Cove
GSSP
FADs
North China
South China
ORDOVICIAN
CAMBRIAN
Cordylodus angulatus
Iapetognathus
Cordylodus lindstromi s.l.
Cordylodus intermedius
Clavohamulus hintzei
Hirsutodontus simplex
Cordylodus proavus
Clavohamulus elongatus
Fryxellodontus inornatus
Hirsutodontus hirsutus
Eoconodontus
Cambrooistodus minutus
Eoconodontus notchpeakensis
Proconodontus muelleri
Iapetognathus fluctivagus
Fauna B
Fauna A
Cordylodus intermedius
Cordylodus andresi
Eoconodontus notchpeakensis
Cordylodus angulatus-Chosonodina herfurthi
Cordylodus lindstromi
Cordylodus intermedius
Cordylodus proavus
Cambrooistodus
Proconodontus
Proconodontus muelleri
C. lindstromi (upper part)-Iapetognathus fluctivagus
Cordylodus lindstromi (lower part)
Eoconodontus
Proconodontus

Fig. 3.

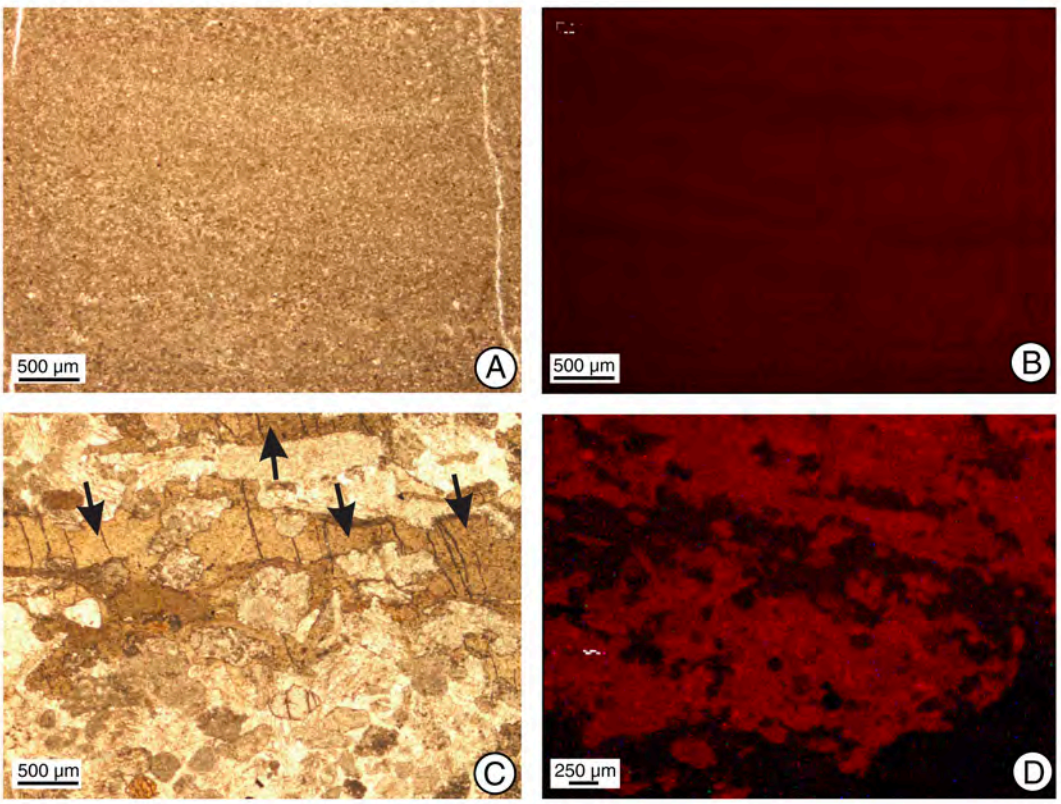
500 µm
A
500 µm
B
500 µm
C
250 µm
D

Fig. 4.

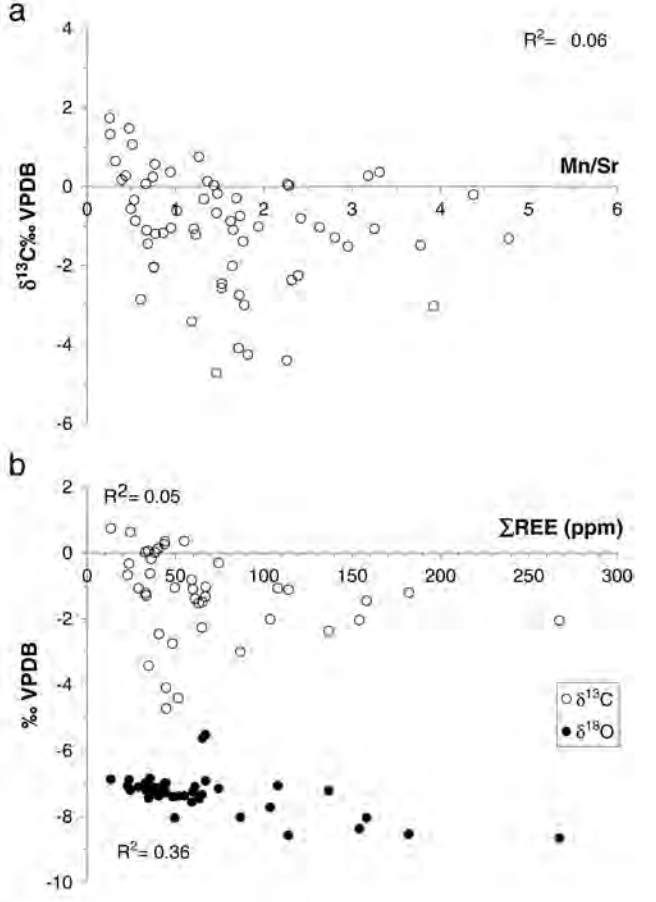
a
R²= 0.06
Mn/Sr
δ13C‰ VPDB
4
2
0
-2
-4
-6
0
1
2
3
4
5
6
b
R²= 0.05
ΣREE (ppm)
‰ VPDB
2
0
-2
-4
-6
-8
-10
0
50
100
150
200
250
300
δ13C
δ18O
R²= 0.36

Fig. 5.

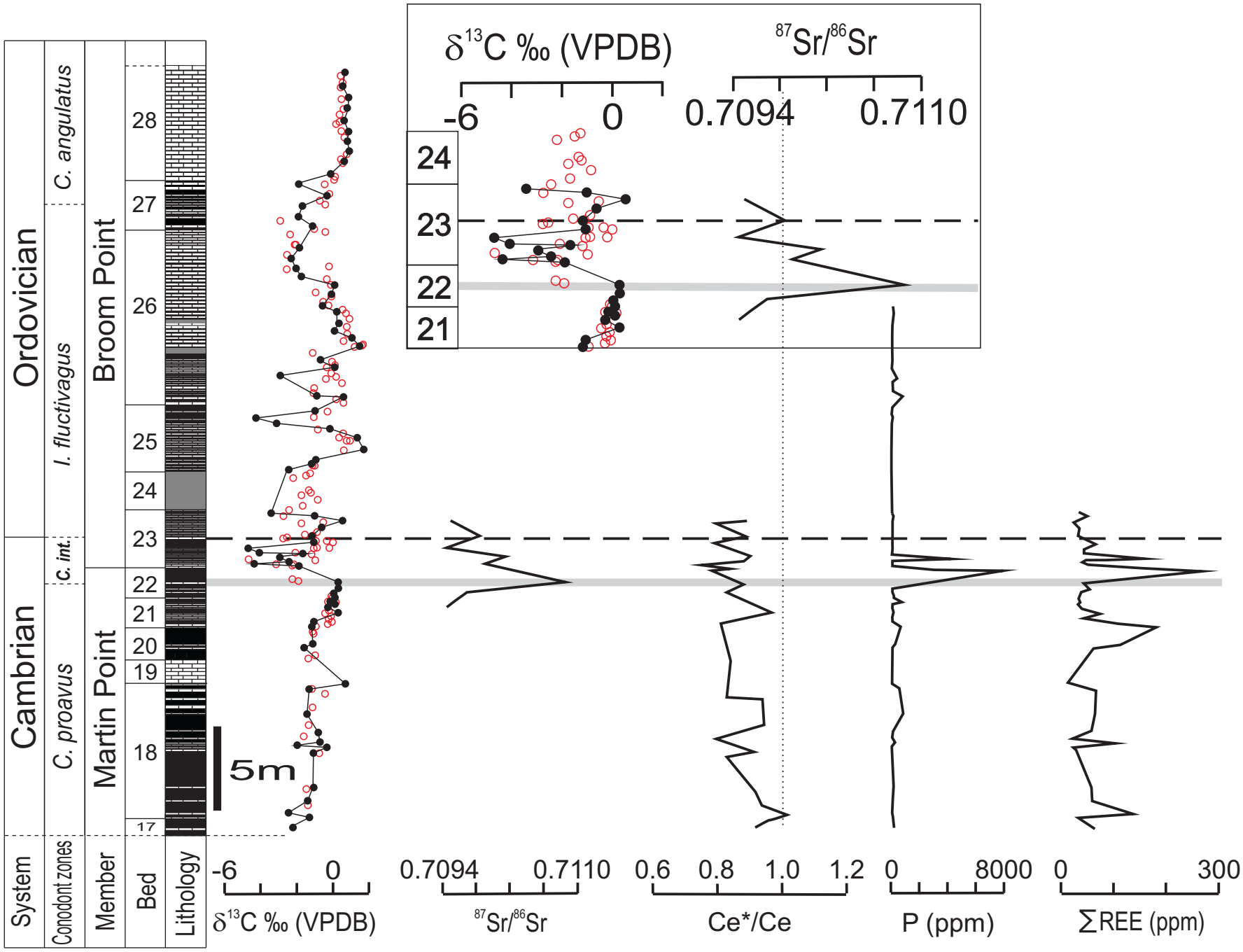
Ordovician
Cambrian
C. angulatus
I. fluctivagus
C. int.
C. proavus
Broom Point
Martin Point
28
27
26
25
24
23
22
21
20
19
18
17
5m
δ13C ‰ (VPDB)
-6
0
87Sr/86Sr
0.7094
0.7110
24
23
22
21
0.6
0.8
1.0
1.2
Ce*/Ce
0
8000
P (ppm)
0
300
ΣREE (ppm)
System
Conodont zones
Member
Bed
Lithology